Cellular/Molecular

Fragile X Mental Retardation Protein Is Required to Maintain Visual Conditioning-Induced Behavioral Plasticity by Limiting Local Protein Synthesis

Han-Hsuan Liu and Hollis T. Cline
Dorris Neuroscience Center, Kellogg School of Science and Technology, The Scripps Research Institute, La Jolla, California 92037

Fragile X mental retardation protein (FMRP) is thought to regulate neuronal plasticity by limiting dendritic protein synthesis, but direct demonstration of a requirement for FMRP control of local protein synthesis during behavioral plasticity is lacking. Here we tested whether FMRP knockdown in *Xenopus* optic tectum affects local protein synthesis *in vivo* and whether FMRP knockdown affects protein synthesis-dependent visual avoidance behavioral plasticity. We tagged newly synthesized proteins by incorporation of the noncanonical amino acid azidohomoalanine and visualized them with fluorescent noncanonical amino acid tagging (FUNCAT). Visual conditioning and FMRP knockdown produce similar increases in FUNCAT in tectal neuropil. Induction of visual conditioning-dependent behavioral plasticity occurs normally in FMRP knockdown animals, but plasticity degrades over 24 h. These results indicate that FMRP affects visual conditioning-induced local protein synthesis and is required to maintain the visual conditioning-induced behavioral plasticity.

Key words: **dendritic protein synthesis; plasticity; retinotectal; visual avoidance behavior; visual conditioning; Xenopus**

Significance Statement

Fragile X syndrome (FXS) is the most common form of inherited intellectual disability. Exaggerated dendritic protein synthesis resulting from loss of fragile X mental retardation protein (FMRP) is thought to underlie cognitive deficits in FXS, but no direct evidence has demonstrated that FMRP-regulated dendritic protein synthesis affects behavioral plasticity in intact animals. *Xenopus* tadpoles exhibit a visual avoidance behavior that improves with visual conditioning in a protein synthesis-dependent manner. We showed that FMRP knockdown and visual conditioning dramatically increase protein synthesis in neuronal processes. Furthermore, induction of visual conditioning-dependent behavioral plasticity occurs normally after FMRP knockdown, but performance rapidly deteriorated in the absence of FMRP. These studies show that FMRP negatively regulates local protein synthesis and is required to maintain visual conditioning-induced behavioral plasticity *in vivo*.

Introduction

Fragile X mental retardation protein (FMRP) is a highly conserved mRNA binding protein expressed throughout the brain (Santoro et al., 2012). Loss of FMRP, as occurs in fragile X syndrome (FXS), is thought to lead to deficits in nervous system function underlying cognitive and behavioral deficits associated with FXS (Liu-Yesucevitz et al., 2011; Darnell and Klann, 2013). Studies in mouse models of FXS and in humans suggest that FMRP regulates sensory system function and plasticity (Kwon et al., 2001; Kogan et al., 2004; Harlow et al., 2010; Kéri and Benedek, 2011; Till et al., 2012; Gandhi et al., 2014). For instance, visual experience increases FMRP expression in visual cortical neurons (Gabel et al., 2004), and loss of FMRP impairs critical period plasticity in the visual, auditory, and somatosensory systems (Dölen et al., 2007; Harlow et al., 2010; Kim et al., 2013), possibly by affecting long-term potentiation (Yang et al., 2014). Loss of FMRP results in exaggerated protein synthesis (Laggerbauer et al., 2001; Li et al., 2001; Qin et al., 2005), which is thought to underlie cognitive deficits seen in FXS. For instance, Fmr1 knock-out mice exhibit increased protein synthesis-dependent mGluR-mediated hippocampal long-term depression (LTD), suggesting that the increased proteins synthesized in the absence of FMRP enhance this type of plasticity (Huber et al., 2000; Bear et al., 2004; Sidorov et al., 2013). Whether such a model generalizes to sensory system plasticity is not yet clear.

Received Nov. 27, 2015; revised May 26, 2016; accepted May 28, 2016.

Author contributions: H.-H.L. and H.T.C. designed research; H.-H.L. performed research; H.-H.L. analyzed data; H.-H.L. and H.T.C. wrote the paper.

This work was supported by National Institutes of Health Grant EY011261, Salk National Eye Institute Core Grant P30 EY019005, and an endowment from the Hahn Family Foundation (H.T.C.). We thank members of the Cline laboratory for discussion and critical comments on this manuscript.

Correspondence should be addressed to Hollis T. Cline, Dorris Neuroscience Center, Kellogg School of Science and Technology, Scripps Research Institute, 10550 North Torrey Pines Road, La Jolla, CA 92037. E-mail: Cline@scripps.edu.

DOI:10.1523/JNEUROSCI.4282-15.2016

 0270-6474/16/367325-15$15.00/0

FMRP and its mRNA targets are packaged in ribonucleoprotein (RNP) granules, which are distributed in neuronal somata, dendrites, and axons and are associated with polyribosomes (Feng et al., 1997; Ling et al., 2004; Weiler et al., 2004; Wang et al., 2014; Faulkner et al., 2015), suggesting that FMRP may regulate neuronal plasticity by negatively regulating protein synthesis downstream of synaptic activity (Feng et al., 1997; Martin et al., 2000; Ling et al., 2004; Weiler et al., 2004; Antar et al., 2005; Sidorov et al., 2013). FMRP-dependent control of protein synthesis in neuronal processes could allow spatiotemporal control over availability of proteins required for plasticity (Liu-Yesucevitz et al., 2011; Darnell and Klann, 2013). Nevertheless, no direct evidence has distinguished FMRP-regulated somatic and local protein synthesis *in vivo*, and no study has demonstrated a specific requirement for FMRP-regulated local protein synthesis in behavioral plasticity in an intact animal.

Here we tested whether FMRP knockdown in *Xenopus* optic tectal neurons affects protein synthesis in neural processes in the tectal neuropil and whether FMRP knockdown affects protein synthesis-dependent visual avoidance behavioral plasticity. Direct investigation of the role of FMRP-regulated local protein synthesis in behavioral plasticity in intact systems has been challenging because it requires methods that can detect low-abundance newly synthesized proteins among the large pool of preexisting proteins and that can minimize contamination of locally synthesized proteins in neuronal processes with somatically synthesized proteins. To address these problems, we optimized the temporal and spatial resolution of fluorescent noncanonical amino acid tagging (FUNCAT; Dieterich et al., 2010; Hinz et al., 2012) in *Xenopus* optic tectum to visualize proteins that are newly synthesized within neural processes in a timeframe consistent with induction and expression of behavioral plasticity (Shen et al., 2014). Under these conditions, we show that protein synthesis in the tectal neuropil increases *in vivo* in response to visual conditioning and with FMRP knockdown. Furthermore, we show that induction of visual avoidance behavioral plasticity occurs normally with FMRP knockdown, but plasticity degrades over 24 h in the absence of FMRP. These results suggest that FMRP normally limits the synthesis of proteins that degrade behavioral plasticity.

Materials and Methods

Animals and transfection. Stage 46–48 albino *Xenopus laevis* tadpoles of either sex were bred in house or purchased (Nasco or *Xenopus* Express) and used for all experiments. The neuronal-specific β-tubulin (NβT)–GFP transgenic tadpoles, which express GFP from the tubulin β class IIb (tubb2b) promoter, were purchased from the National *Xenopus* Resource at the Marine Biological Laboratory. All animal protocols were approved by the Institutional Animal Use and Care Committee of the Scripps Research Institute. Animals were anesthetized by 0.02% MS-222 before injections or electroporation or were terminally anesthetized in 0.2% MS-222. Plasmid constructs (1–2 μg/μl), antisense morpholino oligonucleotides against *fmr1a* (FMOs; 0.1mM; GeneTools) and scrambled control morpholinos (CMOs; 0.1 mM; GeneTools), and cell transfection with electroporation have been described previously (Faulkner et al., 2015).

FUNCAT. L-Azidohomoalaine (AHA) at 500 mM, pH 7.4 (Click Chemistry Tools) colored with ~0.01% fast green was pressure injected into the midbrain ventricle of anesthetized tadpoles. We also mixed AHA with anisomycin (25 μM; Sigma), cycloheximide (50 μM; Sigma), or colchicine (Acros Organics) as stated. Brains were dissected and fixed with 4% paraformaldehyde (PFA) in PBS (pH 7.4), 0.5, 2, 3, or 24 h later, as specified. Samples were processed for click chemistry according to the following protocol, modified from previous studies (Dieterich et al., 2010; Hinz et al., 2012). Permeabilized whole-mount brains or vibratome sections were transferred to Eppendorf tubes or six-well plates with reaction mixture composed of 100 μM Tris [(1-benzyl-1H-1,2,3-triazol-4-yl)methyl]amine (TBTA, Sigma) dissolved in 4:1 tBuOH/DMSO (Sigma), 100 μM CuSO4 (Sigma), 1.25 μM Alexa Fluor 488 alkyne (Invitrogen), and 250 μM Tris(2-carboxyethyl)phosphine (TCEP, Sigma). The reaction proceeded overnight at room temperature. Samples were washed several times and then either cleared and mounted in 50% glycerol/6 M urea and imaged with an Olympus FluoView500 confocal microscope with a 20× [0.8 numerical aperture (NA)], 40× (1.0 NA), or 60× (1.4 NA) oil-immersion lens or processed for immunohistochemistry as described below.

Immunohistochemistry and quantification. Tadpoles were anesthetized in 0.02% MS-222 solution and fixed with 4% PFA in PBS, pH 7.4, overnight at 4°C for immunolabeling with anti-Sox2 antibodies or anti-NβT antibodies. To immunolabel with anti-vimentin antibodies, animals were fixed with 100% methanol overnight at −20°C or 2% PFA for 1 h at room temperature, followed by 100% methanol overnight at −20°C. To immunolabel with anti-GABA antibodies, we fixed animals with 4% PFA and 1% glutaraldehyde overnight at 4°C. Brains were dissected and either processed as whole brains or sectioned at 40 μm on a vibratome. Samples were permeabilized and blocked in 4% BSA and 1% normal goat serum in 0.5% Triton X-100 for 1 h at room temperature and then incubated in 1:200 mouse anti-β-tubulin I+II (T8535; Sigma; Moody et al., 1996), 1:200 rabbit anti-Sox2 [2748S (recognizes *Xenopus* Sox2 and Sox3); Cell Signaling Technology; Gaete et al., 2012)], 1:1000 rabbit anti-GABA (A2052; Sigma; Li and Cline, 2010), or 1:50 mouse anti-vimentin (14h-7; Developmental Studies Hybridoma Bank; Dent et al., 1989) overnight at 4°C, followed by 2 h in 1:200 anti-mouse Alexa Fluor 647 or anti-rabbit Alexa Fluor 647 (Life Technologies) at room temperature. Samples were cleared and mounted in 50% glycerol/6 M urea and imaged with an Olympus FluoView500 confocal microscope with a 20× (0.8 NA) or 60× (1.4 NA) oil-immersion lens or on a Nikon A1 confocal microscope with a 60× (1.4 NA) oil-immersion lens.

Fluorescence intensity of AHA labeling in the cell body layer or in the neuropil was quantified in single optical sections from confocal *z* series through the brain using custom applications created in MATLAB 2009b (MathWorks, Psychophysics Toolbox extensions). We selected the most dorsal optical section through the optic tectum ventral to the anterior commissure from the confocal *z* stacks and oriented the brain image along the rostrocaudal axis. Only samples in which the ventricle is closed at the dorsal midline were included in the analysis. We manually drew a dorsoventral line 40–60 pixels long (24.8–37.2 μm) along the midline, extending caudally from the anterior commissure, and randomly plotted 10 mediolateral lines perpendicular to the midline. We calculated the average fluorescence intensity along the 10 mediolateral lines from the midline through the cell body layer to the neuropil in both the left and right tectal lobes. The ventricular cell body layer is enriched for neural progenitor cells (NPCs), identified by Sox2 immunolabeling, and neurons, identified by NβT labeling, are lateral to the NPCs. Samples with >10% difference in total fluorescence intensity between the left and right hemispheres were excluded from the analysis. Fluorescence intensity in the cell body layer was measured in the 50 pixels (31 μm) to the left and right of the midline, and the neuropil was measured between 80 and 100 pixels (49.6–68.2 μm) to the left and right of the midline.

To test whether AHA-labeled proteins are enriched in cell types or cellular compartments labeled by the different markers, we created masks of regions of interest (ROIs) based on immunolabeling with Sox2, GABA, and NβT in the cell body layer or neuropil. The average AHA labeling intensities per unit area within or outside of the masks were normalized to average AHA intensity within ROIs without masking.

For quantification of NβT-immunolabeled neuronal processes in Figure 3, we used the 2D Sholl analysis plugin in Fiji (Ferreira et al., 2014). We determined the numbers of intersections of NβT-immunolabeled neuronal processes with rings of increasing radius extending from the neuropil in the left top corner through the cell body layer in the right bottom corner in the *z* projections of images of NβT immunolabeling in the optic tectum 0.5 and 2 h after PBS or colchicine injection. Mean intersections (see Fig. 3*e*) are the average of intersections at all rings.

To quantify the effect of FMRP knockdown on translation, we electroporated tadpole midbrains with CMOs or FMOs and, 2 d later, injected the midbrain ventricle with AHA, as described above. Animals were terminally anesthetized and fixed 1 or 3 h later and processed for click chemistry, as described above. A single experiment included animals from a single clutch of embryos processed together, blind to treatment. Fluorescence intensity in the NPC layer was measured in the 20 pixels (12.4 μm) to the left and right of the midline, and the neuronal cell layer measurement was made from the 30 pixels (18.6 μm) just lateral to the NPC layer. The average fluorescence intensities of animals with 3 h AHA labeling were then normalized to the average intensities of animals with 1 h AHA labeling from the same experiment. The AHA intensity ratio 3 h/1 h of CMO- or FMO-treated animals from each independent experiment was paired for statistic analysis.

For quantification of AHA-labeled proteins in neuronal processes within the optic tectal neuropil, we developed and performed customized image analysis macros in NIH ImageJ. We used NβT immunolabeling as a mask to identify neuronal processes and measured AHA fluorescence intensity only in the NβT mask within a fixed ROI of 1762.66 μm^2 in the tectal neuropil (see Fig. 5), propagated through the *z* series of the tectal neuropil. The final fluorescence intensity value for each animal was an average from image stacks of two or more representative 40-μm-thick sections. The AHA fluorescence intensity of the experimental group was normalized to the control group within each independent experiment and then pooled for statistic analysis.

All samples were prepared, imaged, and analyzed in parallel, blind to treatment, using the same image acquisition and analysis settings. Figures were compiled using Adobe Illustrator (Adobe Systems).

In vivo *time-lapse imaging and analysis of NβT–GFP transgenic tadpoles.* NβT–GFP transgenic tadpoles were imaged on a custom-built two-photon microscope with a 20× water-immersion lens (0.95 NA). To reduce interference from pigment cells in the skin, we raised tadpoles in 0.001% phenylthiourea (Sigma) starting 2–3 d after fertilization until stage 47/48 when they were used for experiments. We collected time-lapse images of optic tecta before, 0.5 h, and 2 h after injecting the midbrain ventricle with ~10 nl of PBS or 5 or 10 mg/ml colchicine. All images were collected using the same image acquisition settings.

To compare the change in cell morphology of NβT–GFP-expressing neurons in Figure 3*b*, we measured the complexity of the GFP-labeled neuronal processes using Fuji 3D Sholl analysis. We counted the numbers of intersections of NβT–GFP neuronal processes with rings of increasing radius at 100, 150, 200, 250, and 300 μm extending from the neuropil in the left top corner through the cell body layer in the right bottom corner in the *z* projections of images of NβT–GFP. The mean intersections are the average of intersections at all radii (see Fig. 3*a*). The values for each time point for each animal were normalized to the value before PBS or colchicine injection. The normalized value for each time point from individual animals was paired for statistic analysis.

In vivo *time-lapse imaging and analysis of cytoplasmic polyadenylation element binding protein–CFP RNPs and mitochondria.* We determined the effect of colchicine on the distribution of cytoplasmic polyadenylation element binding protein (CPEB)-CFP-labeled RNP granules (see Fig. 4) as follows: Optic tecta were sparsely transfected with cytosolic yellow fluorescent protein (YFP) and CPEB-CFP and, after 3 d, were imaged on a PerkinElmer Ultraview Vox spinning disk confocal microscope with a 25× water-immersion lens (1.1 NA) at stated times after ventricular injection with colchicine or PBS. To image YFP and CFP, we sequentially excited YFP and CFP with 488 or 405 nm laser lines, respectively, and imaged with UltraVIEW emission filters "527(W55)" or "485(W60)" accordingly. To quantify CPEB–CFP RNP granules, we used the 3D object counter plugin in NIH ImageJ (Bolte and Cordelieres, 2006). We set the threshold intensity to 150 and counted objects larger than 0.25 μm^3 within YFP^+ areas. Then we assigned each object to an individual cell in the original images.

To determine the effect of colchicine on the distribution of mitochondria (see Fig. 3*d–g*), stage 47/48 tadpoles received ventricular injections of 50 μM MitoTracker DeepRed FM (Invitrogen) diluted in PBS from 1 mM stock solution in DMSO mixed with PBS or colchicine. Time-lapse confocal *z* series through the optic tectum were collected at the stated times on a PerkinElmer Ultraview Vox spinning disk confocal microscope with a 25× water-immersion lens (1.1 NA). The fluorescence intensity of MitoTracker labeling was measured in an ROI of the cell body layers and an ROI of the neuropil along the mediolateral extent of the tectum in three individual optical sections per brain at each time point. The ROIs were 150 × 100 pixels (43.86 × 29.24 μm) positioned at the ventricular and pial edges of the tectal lobe (see Fig. 3*b*). Each fluorescence intensity value is the average from three sections per tectal lobe. The average fluorescence intensities from the 0.5 and 2 h time points were normalized to the intensities at the 0 h time point for each animal. The normalized MitoTracker labeling intensity from each time point from individual animals was paired for statistic analysis.

Visual conditioning and visual avoidance assay. Visual conditioning was provided to animals as described previously (Shen et al., 2014). Animals were exposed to moving bars (1 cm width; 0.3 Hz; luminance, 25 cd/m^2) continuously for 1.5 h. The visual avoidance assay was conducted as reported previously (Dong et al., 2009; Shen et al., 2014). Briefly, four to six tadpoles were placed in a 8 × 3 cm tank filled with ~25 ml of Steinberg's rearing solution. The bottom of the chamber was mounted with a backprojection screen. Visual stimuli were projected on the screen using a microprojector (MPro110; 3M). Videos of tadpoles illuminated by infrared LEDs were recorded with a Hamamatsu ORCA-ER digital camera. Visual stimuli were generated and presented by MATLAB 2009b. Randomly positioned moving spots of 0.4 cm diameter were presented in pseudorandom order for 60 s. Visual avoidance behavior was scored as a change in swim trajectory or speed and plotted as an avoidance index (AI), the ratio of avoidance responses to the first 10 encounters with an approaching visual stimulus. Animals in which >50% of turning events were independent of an encounter with visual stimuli were not included for additional analysis. Outliers, defined as those with AI greater that two SDs from the mean, were excluded from the analysis.

Statistical tests. All data are presented as mean ± SEM based on at least three independent experiments unless otherwise noted. Data are considered significantly different when p values are <0.05. The nonparametric Mann–Whitney *U* or Wilcoxon's signed-rank tests were used to compare between two independent groups or matched pairs as stated. The Steel–Dwass test was used for nonparametric multiple comparisons between all pairs. The Wilcoxon's test was used for nonparametric multiple comparisons for each pair. Experiments and analysis were performed blind to the experimental conditions. JMP 11 statistics software (SAS Institute) was used for all statistics analysis.

Results

FUNCAT detects rapid changes in translation in intact animals

FUNCAT allows visualization of newly synthesized proteins after incorporation of a noncanonical amino acid, such as AHA, a methionine analog, in place of endogenous methionine. Click chemistry is then used to tag a bio-orthogonal group with a fluorescent reporter. Previous studies applied FUNCAT to intact zebrafish and showed that exposing animals to AHA in rearing solution over a period of several days labeled proteins throughout the animal without toxicity or behavioral impairment (Hinz et al., 2012). We have shown that AHA injection into the brain ventricle allows rapid labeling of newly synthesized proteins over the time course of hours using biotin-based bio-orthogonal noncanonical amino acid tagging (BONCAT) on dot blots (Shen et al., 2014). Here we tested whether ventricular injection of AHA improves the temporal resolution of FUNCAT in *Xenopus* optic tectum *in vivo*. AHA was injected into the midbrain ventricle, and brains were dissected and processed for click chemistry to tag AHA with fluorophore for visualization of AHA-labeled proteins. Figure 1*a* shows an example of AHA labeling detected 3 h after ventricular injection next to a sketch of the tadpole midbrain with the tectal cell body layer and neuropil shaded in green and gray, respectively. AHA labeling was detected 2 h after injection of AHA compared with minimal background labeling after

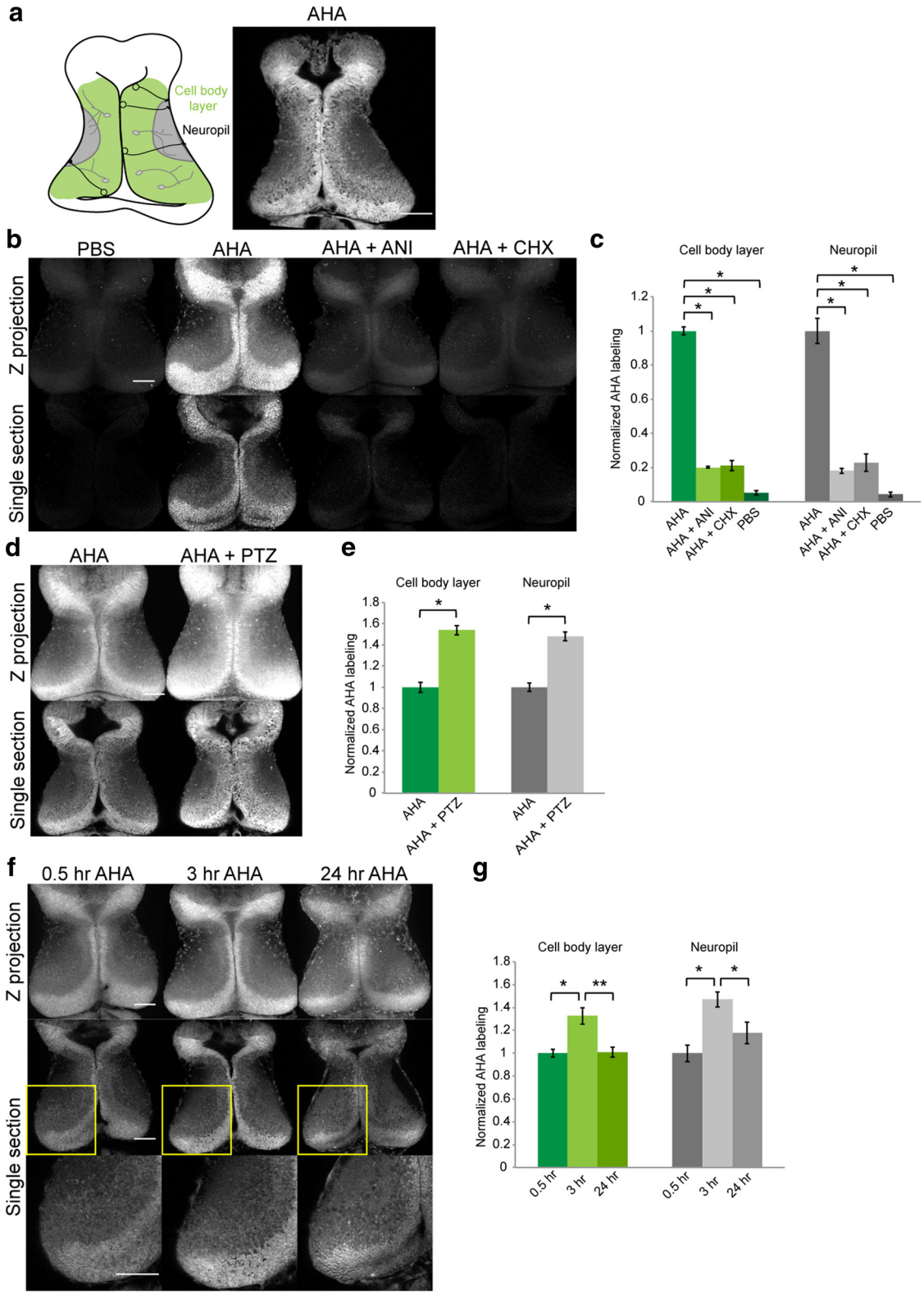

Figure 1. FUNCAT reveals rapid changes in protein synthesis in intact animals. ***a***, Left, Schematic of tadpole optic tectum showing the location of cell body layer (green), which includes NPCs (black) and neurons (gray) extending processes into the neuropil (gray). Right, Image of whole-mount brain processed for click chemistry with Alexa Fluor 488 –alkyne to visualize newly synthesized proteins 3 h after ventricular injection of AHA. ***b***, ***d***, ***f***, Images of fluorescent AHA labeling in single confocal optical sections from comparable depths across groups or *z* projections through optic tectum. ***b***, *In vivo* AHA labeling detected after 2 h ventricular AHA injection is blocked by anisomycin (ANI, 25 μM) and cycloheximide (CHX, 50 μM). ***c***, Normalized AHA labeling in the cell body layer and neuropil in animals treated with PBS, AHA, AHA plus ANI, or AHA plus CHX. AHA: 1 $\pm$ 0.02 in cell body layer and 1 $\pm$ 0.07 in neuropil, $n = 10$ brains; ANI: 0.2 $\pm$ 0.004 in cell body layer and 0.18 $\pm$ 0.01 in neuropil, $n = 4$ brains; CHX: 0.21 $\pm$ 0.03 in cell body layer and 0.23 $\pm$ 0.05 in neuropil, $n = 5$ brains; PBS: 0.05 $\pm$ 0.01 in cell body layer and 0.04 $\pm$ 0.01 in neuropil, $n = 5$ brains. ***d***, Tadpoles exposed to PTZ (15 mM) in rearing solution for 2 h after AHA injection have more intense AHA labeling. ***e***, Normalized AHA labeling in the cell body layer and neuropil in animals exposed to PTZ compared with controls. 2 h AHA: 1 $\pm$ 0.05 in cell body layer and 1 $\pm$ 0.04 in neuropil, $n = 3$ brains; 2 h AHA + PTZ: 1.54 $\pm$ 0.05 in cell body layer and 1.48 $\pm$ 0.04 in neuropil, $n = 3$ brains. ***f***, *In vivo* AHA labeling detected 0.5, 3, or 24 h after AHA injection. Bottom row shows enlargements of yellow boxed areas in the middle row. (***g***) Normalized (*Figure legend continues.*)

PBS injection (Fig. 1*b*,*c*). Coinjection of AHA with the translational inhibitors anisomycin (25 μM) or cycloheximide (50 μM) significantly decreased AHA labeling seen over 2 h (Fig. 1*b*,*c*). When animals were treated with 2 h bath application of 15 mM pentylenetetrazol (PTZ), a GABA receptor antagonist that increases brain activity, AHA labeling was significantly greater in both the tectal cell body layer and neuropil, indicating a similar proportional increase in activity-induced protein synthesis in the cell bodies and processes (Fig. 1*d*,*e*). We compared the intensity of AHA labeling in the neuropil to the cell body layer and found that the neuropil has 18.8 ± 0.35% of AHA labeling intensity in the cell body layer under control conditions and 18.1 ± 0.98% after PTZ treatment, indicating that PTZ increased protein synthesis to a comparable extent in the cell body layer and neuropil. These data show that FUNCAT has sufficient sensitivity to detect changes in protein synthesis in the cell body layer and neuropil within a 2 h window when animals are exposed to drugs that either block translation or indirectly increase protein synthesis downstream of increased neuronal activity.

Next, we tested whether shorter AHA labeling times could be used to visualize newly synthesized proteins with FUNCAT and how long AHA-labeled proteins can be detected to identify the temporal resolution of FUNCAT *in vivo*. We detected AHA-labeled proteins as soon as 0.5 h after AHA injection into the midbrain ventricle, and AHA labeling increased over 3 h after injection in both the cell body layer and neuropil. When the animals were fixed 24 h after AHA injection, AHA-labeled proteins could still be detected (Fig. 1*f*,*g*). These data indicate that newly synthesized proteins can be detected in live animals as soon as 0.5 h after AHA injection and that they persist for at least 1 d.

We combined FUNCAT with immunohistochemistry for cell-type-specific markers to determine whether AHA labeling differed in different cell types. We observed higher-intensity AHA labeling in the ventricular layer cells that are labeled by Sox2 antibodies, a marker of NPCs, indicating more active protein translation in NPCs than in neurons. We quantified the intensity of AHA labeling in Sox2$^+$ cells compared with Sox2$^-$ cells using a mask based on the Sox2 immunolabeling, as described in Materials and Methods. This analysis indicated that AHA labeling is significantly enriched in Sox2$^+$ cells (Fig. 2*a*; Table 1). Note that the Sox2 mask only measures AHA in the NPC nuclei, whereas AHA labeling is both nuclear and cytosolic, so the AHA enrichment in NPCs is an underestimate. AHA labeling is comparable in GABA-immunopositive and GABA-immunonegative neurons and processes in both the cell body layer and the neuropil (Fig. 2*b*; Table 1). AHA-labeled proteins were detected not only in the cytosol, where translation occurs, but also in the nuclei, consistent with translocation of newly synthesized proteins from the cytosol to the nuclei (Fig. 2*a*,*b*). We also observed AHA labeling along the processes of NPCs and neurons, marked by antibodies against vimentin and NβT (Moody et al., 1996), respectively. The vimentin labeled radial glial NPC processes were too fine to quantify AHA labeling reliably (Fig. 2*c*). By analyzing the intensity of AHA labeling per unit area in a mask of NβT$^+$ labeling compared with NβT$^-$ labeling, we found that AHA labeling is significantly enriched in NβT$^+$ processes in the cell body layer compared with the NβT$^-$ area (Fig. 2*d*; Table 1). It is unclear whether the AHA-labeled proteins localized in processes were synthesized locally or were synthesized in the somata and then transported to the processes.

Visualization of locally synthesized protein in neural processes *in vivo*

The goal of our study is to test whether FMRP regulates local protein synthesis in neuronal processes *in vivo* and whether FMRP-regulated protein synthesis is required for behavioral plasticity. Specific visualization of locally synthesized proteins within neural processes has been a challenge in intact animals because it has been difficult to segregate locally synthesized proteins from proteins that are synthesized in the cell body and transported to the processes. One way to tackle this problem is to block the cellular machinery required to transport newly synthesized proteins from the somata to the processes. Previous studies used colchicine, which inhibits microtubule polymerization, to block microtubule-dependent transport from the somata to the processes (Fischer and Schmatolla, 1972; Shan et al., 2003; Antar et al., 2005). For our purposes, we wanted to disrupt microtubules to interfere with protein transport from the somata but preserve the presence of RNP granules in neural processes, thereby maintaining the cellular machinery required for protein synthesis in processes. In preliminary experiments, we imaged transgenic *Xenopus* tadpoles expressing GFP driven by the neuron-specific β-tubulin class IIb (NβT or tubb2b) promoter in all neurons before and after ventricular injection of ~10 nl of 5 or 10 mg/ml colchicine or PBS. These experiments suggested that treatment with 5 mg/ml colchicine might affect microtubule stability (data not shown). Furthermore, ventricular injections of dilute fast green dye show that small molecules are rapidly cleared from the brain ventricle, suggesting that ventricular colchicine may have a transient effect on microtubule structure. To address this directly, we tested whether microtubule structure could be disrupted by ventricular injection of colchicine, using immunolabeling with antibodies against NβT (Moody et al., 1996). Animals received ventricular injections of PBS or 5 mg/ml colchicine and were fixed 0.5 or 2 h later. As also seen in Figure 2, NβT immunolabeling identifies bundles of microtubules in neuronal processes extending from cell bodies into the neuropil in PBS-injected control animals (Fig. 3*a*,*b*). Microtubule bundles were disorganized 0.5 h after colchicine treatment, and this effect was reversed after 2 h (Fig. 3*a*,*b*), likely because the colchicine was cleared from the ventricle. Sholl analysis indicated that the integrity of NβT-labeled processes extending from the cell body layer to the neuropil decreased 0.5 h after colchicine and recovered to control values at 2 h (Fig. 3*c*).

Next, we examined whether microtubule-dependent transport from neuronal cell bodies into processes was affected by ventricular colchicine injection by tracking the distribution of mitochondria in the tectum (Plucińska et al., 2012). We labeled mitochondria by coinjecting MitoTracker with either PBS or 5 mg/ml colchicine into the midbrain ventricle and collected *in vivo* time-lapse confocal images of the optic tecta immediately after (0 h) and 0.5 and 2 h after injection. Figure 3*d* shows the location of the imaged portion of the tectum. Images in Figure 3, *e* and *f*, are inverted such that fluorescently labeled mitochondria appear black. We measured the fluorescence intensity across the tectum from the pial layer through the neuropil to the cell body layer, abutting the ventricle (Fig. 3*e*, bottom). MitoTracker quickly labels mitochondria in the cell body layer, and analysis of

←

(*Figure legend continued.*) AHA labeling in the cell body layer and neuropil in animals injected with AHA and fixed at different time points as stated. 0.5 h: 1 ± 0.03 in cell body layer and 1 ± 0.07 in neuropil, $n = 4$ brains; 3 h AHA: 1.33 ± 0.07 in cell body layer and 1.47 ± 0.07 in neuropil, $n = 9$ brains; 24 h AHA: 1 ± 0.04 in cell body layer and 1.18 ± 0.09 in neuropil, $n = 9$ brains. *$p < 0.05$, **$p < 0.01$, Steel–Dwass test for all pairs or Mann–Whitney *U* test for two groups. Error bars represent ± SEM. Scale bar, 100 μm.

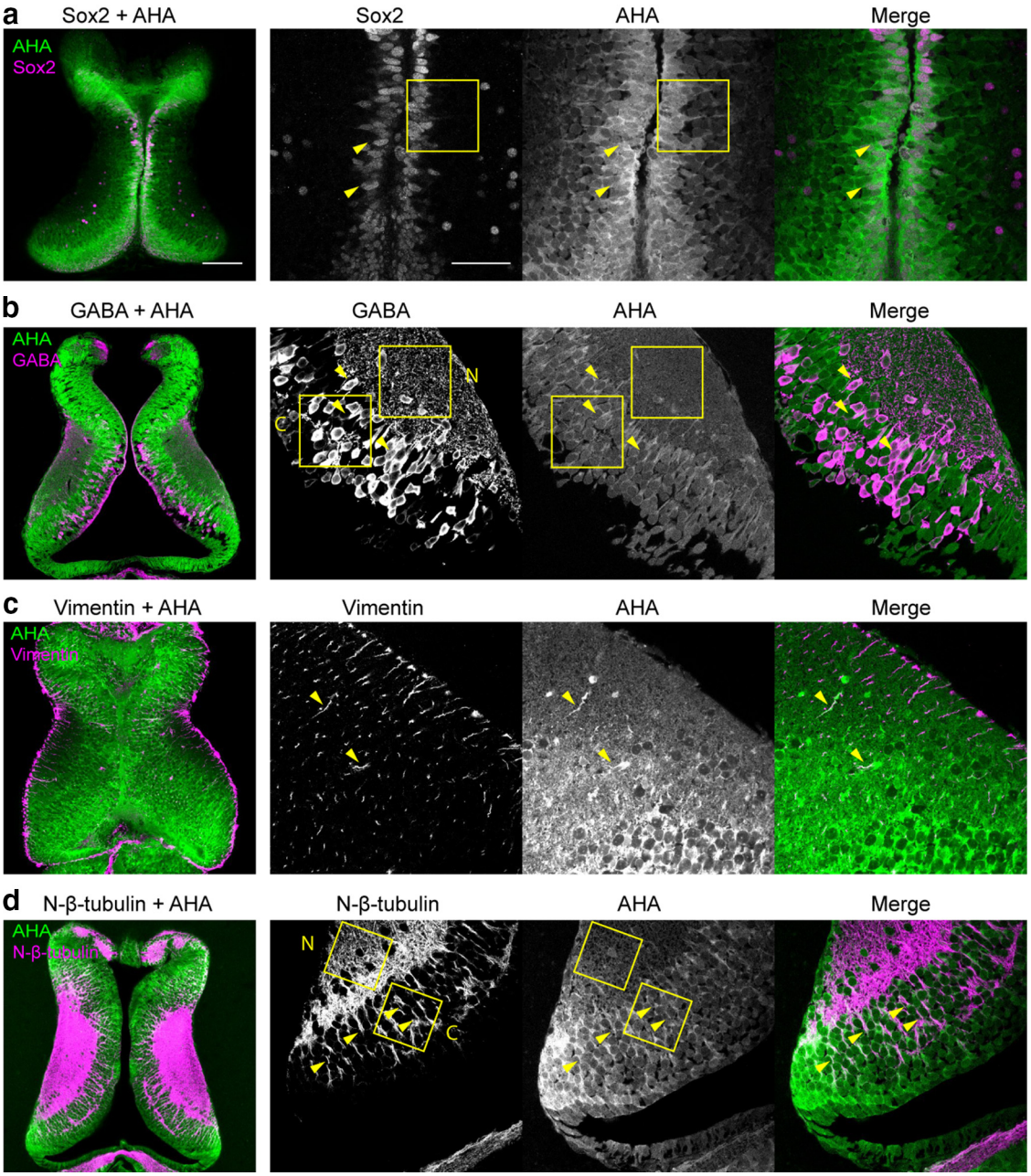

Figure 2. Cellular distribution of newly synthesized proteins in the tadpole tectum. ***a–d***, Single optical sections of AHA labeling (green) and immunolabeling (magenta) targeting Sox2 (***a***), GABA (***b***), vimentin (***c***), or NβT (***d***). Brains were fixed and processed to visualize AHA labeling 3 h after injecting AHA into the brain ventricle. Sox2 and vimentin immunolabeling were performed on whole brains after FUNCAT (***a***, ***c***). GABA and NβT immunolabeling was done in 40 μm sections (***b***, ***d***). Yellow arrowheads mark the colocalization of AHA labeling with different markers. Images in the left columns are from different animals than the higher-magnification series to the right. AHA labeling intensity was measured in the yellow boxed areas (see Table 1). C, Cell body layer; N, neuropil. Scale bars: left column, 100 μm; right three columns, 50 μm.

Table 1. AHA labeling intensity in NPCs, neurons, and processes

	Mean ± SEM		Mann–Whitney *U* test (*p* value)	
	Cell bodies	Neuropil	Cell bodies	Neuropil
Sox2 $^{+}$	1.63 ± 0.04		$p < 0.01$	
Sox2 $^{-}$	0.84 ± 0.01			
GABA $^{+}$	1.08 ± 0.02	1.04 ± 0.02	$p < 0.01$	$p < 0.01$
GABA $^{-}$	0.98 ± 0.01	0.98 ± 0.01		
NβT $^{+}$	1.23 ± 0.03	1.00 ± 0.06	$p < 0.01$	$p = 0.81$
NβT $^{-}$	0.94 ± 0.09	0.99 ± 0.03		

AHA labeling (intensity/pixel) in masks created from Sox2, GABA, or NβT immunolabeling positive and negative regions was normalized to total AHA labeling. The nonparametric Mann–Whitney *U* test was used to compare normalized average AHA labeling between groups. $n = 6$ for all comparisons.

in vivo time-lapse images from control tecta indicates that the density of mitochondria in the cell body layer and neuropil increases over 2 h after PBS injection (Fig. 3*f*,*g*). In contrast, *in vivo* images collected 0, 0.5, and 2 h after 5 mg/ml colchicine treatment indicate that the density of mitochondria increases in the cell body layer but not in the neuropil (Fig. 3*f*,*g*). MitoTracker labeling intensity in the cell body layer and neuropil was comparable immediately after PBS and colchicine treatment [cell body layer: PBS, 4005 ± 607 arbitrary units (AU); colchicine, 4920 ± 369 AU; neuropil: PBS, 1452 ± 141 AU; colchicine, 1360 ± 101 AU; $n = 9$ brains for PBS and colchicine]. After 2 h, MitoTracker labeling intensity in the neuropil of PBS-treated animals was

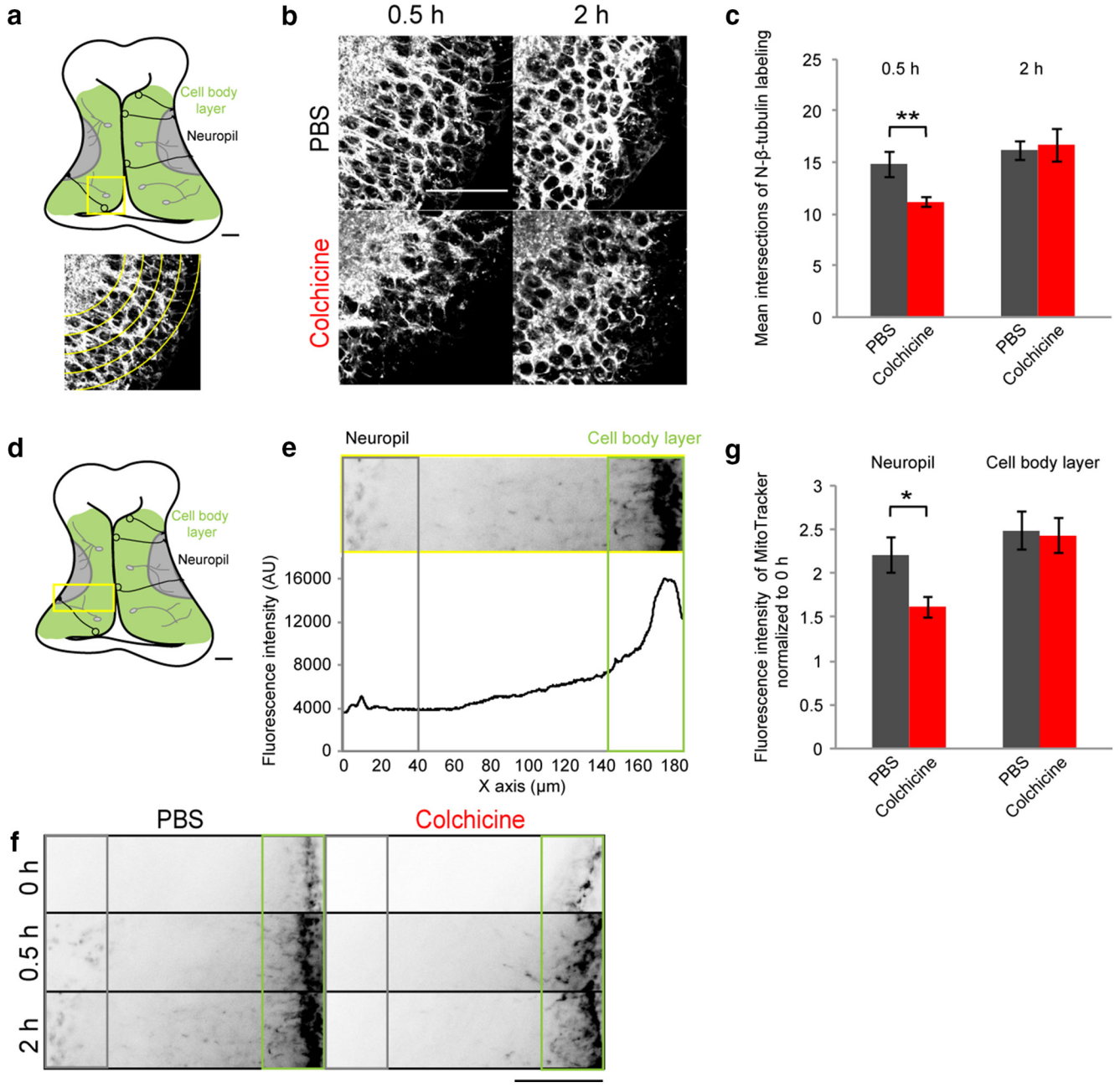

Figure 3. Colchicine affects microtubule structure and microtubule-dependent mitochondria transport. ***a***, Top, Schematic of the optic tectum with a yellow box marking the location of images shown in ***b***. Bottom, Schematic of Sholl analysis used to analyze NβT immunolabeling in ***b***. ***b***, Representative *z* projections of NβT immunolabeling in the optic tectum 0.5 and 2 h after injection of PBS or colchicine into the midbrain ventricle. Colchicine decreases the integrity of microtubule bundles labeled with NβT antibodies at 0.5 h, but this appears to be reversed at 2 h. ***c***, Sholl analysis quantifying the mean intersections of NβT labeling with arcs of increasing radium 0.5 and 2 h after PBS or colchicine injection. PBS: 14.80 $\pm$ 1.24 at 0.5 h, n = 5 brains and 16.11 $\pm$ 0.89 at 2 h, n = 9 brains; colchicine: 11.17 $\pm$ 0.48 at 0.5 h, n = 6 brains and 16.67 $\pm$ 1.61 at 2 h, n = 6 brains. ***d***, Schematic of the optic tectum with a yellow box marking the location of images shown in ***e*** and ***f***. ***e***, Top, Inverted *z* projection of an *in vivo* image of MitoTracker labeling in the optic tectum. The ventricle is to the right, and pia is to the left. Boxed regions show ROIs of the portion of the neuropil and cell body layer in which MitoTracker labeling intensity was measured. Bottom, Fluorescence intensity measured in the image shown and in the ROIs corresponding to neuropil and cell body ROIs. ***f***, Representative inverted *z* projections of mitochondria labeled by MitoTracker 0, 0.5, and 2 h after coinjection with PBS or colchicine. ***g***, Colchicine decreases the MitoTracker labeling intensity in the neuropil ROI compared with PBS. PBS: 2.49 $\pm$ 0.22 in cell body layer and 2.21 $\pm$ 0.20 in neuropil, n = 9 brains; colchicine: 2.43 $\pm$ 0.20 in cell body layer and 1.61 $\pm$ 0.12 in neuropil, n = 9 brains. $^{*}p < 0.05$, $^{**}p < 0.01$, Mann–Whitney *U* test. Error bars represent $\pm$ SEM. Scale bar, 50 μm.

significantly greater than in colchicine-treated animals (Fig. 3*f*,*g*). Labeling in the cell body layer was comparable in PBS- and colchicine-treated animals, indicating that MitoTracker uptake into the cells was not affected (Fig. 3*f*,*g*). These results indicate that microtubule-dependent transport from neural cell bodies into processes is decreased by ventricular colchicine injection.

To examine whether the cellular machinery required for protein synthesis is retained in processes after colchicine treatment, we labeled RNP granules and visualized cells by coexpressing CPEB–CFP fusion protein and cytosolic YFP (Bestman and Cline, 2009). We did not label RNP granules with FMRP fusion proteins because overexpressing FMRP causes apoptosis in NPCs and decreases dendritic arbor elaboration in neurons (Faulkner

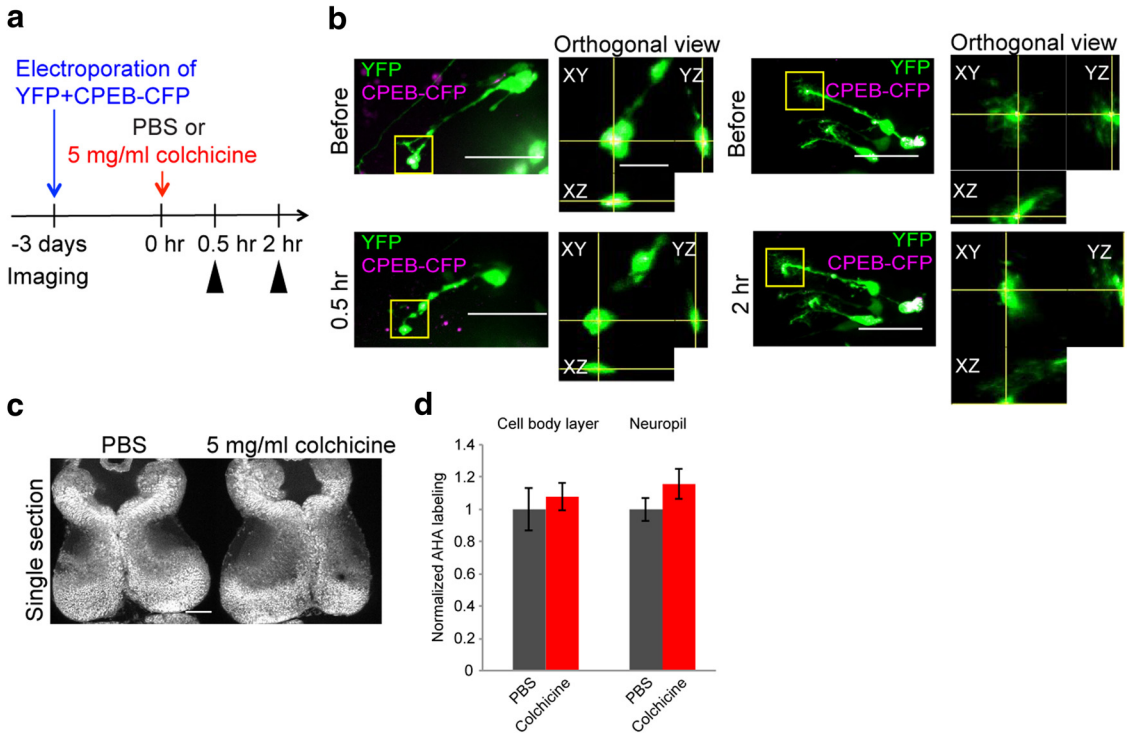

Figure 4. Colchicine does not affect distribution of RNP puncta or FUNCAT. ***a***, Protocol to image RNP granules in colchicine-treated tadpoles. Tadpoles were electroporated with a bidirectional plasmid expressing cytosolic YFP and CBEP–CFP to visualize RNP granules in tectal cells. After 3 d, animals were injected in the midbrain ventricle with colchicine and imaged on a confocal microscope before injection and 0.5 or 2 h later. ***b***, Representative *z* projections of *in vivo* time-lapse confocal images of tectal cells labeled by expression of cytosolic YFP and CPEB–CFP collected before colchicine injection and 0.5 and 2 h later. CPEB–CFP-labeled RNP granules are present in the neural process throughout the colchicine treatment. Rights columns are single optical sections of the boxed areas in the left column including orthogonal views. ***c***, Ventricular colchicine injection does not affect AHA labeling. Images of a single representative optical section of the whole-mount brain from tadpoles injected with AHA in 5 mg/ml colchicine or PBS. After 1.5 h, brains were processed for click chemistry and AHA labeling to visualize newly synthesized proteins. ***d***, Normalized AHA labeling in cell body layer and neuropil in animals injected with AHA or AHA plus colchicine. PBS: 1 ± 0.13 in cell body layer and 1 ± 0.07, $n = 5$ brains; 5 mg/ml colchicine: 1.08 ± 0.08 in cell body layer and 1.16 ± 0.09, $n = 4$ brains. $^*p < 0.05$, Mann–Whitney *U* test. Error bars represent ± SEM. Scales bars: ***b*** left column, 50 μm; ***b*** right column, 10 μm; ***c***, 100 μm.

Table 2. Change in number of CPEB–CFP granules with colchicine treatment

	Before		After	
	Mean ± SEM	Range	Mean ± SEM	Range
0.5 h	2.33 ± 0.33	2–3	1.67 ± 0.33	1–6
2 h	3.33 ± 0.71	1–2	5.83 ± 2.24	1–16

Change in number of CPEB–CFP granules with colchicine treatment. CPEB–CFP granules larger than 0.25 μm^3 within YFP $^+$ cells were quantified using 3D object counter. The mean ± SEM and ranges of CPEB–CFP granules before and after 0.5 h ($n = 3$ cells) and 2 h ($n = 6$ cells) colchicine treatment are shown.

et al., 2015). Three days later, we injected PBS or 5 mg/ml colchicine into the midbrain ventricle and collected *in vivo* confocal images of labeled optic tectal cells before and 0.5 and 2 h after colchicine or PBS injection (Fig. 4*a*). We identified CPEB–CFP puncta in YFP-expressing cells based on orthogonal views of *x*, *y*, *z* confocal images (Fig. 4*b*). All of the cells with CPEB–CFP-labeled RNP granules at the first time point retained them in both colchicine- and PBS-injected animals (Table 2). We next tested whether ventricular injection of colchicine affects AHA labeling and found that the intensity of AHA labeling in the tectal cell body layer and neuropil was comparable in animals 0.5 h after ventricular injection with PBS or colchicine (Fig. 4*c*,*d*), indicating that colchicine treatment does not interfere with protein synthesis. Together, these data indicate that ventricular injection of 5 mg/ml colchicine transiently disrupts microtubule structure and microtubule-dependent transport from the somata into neural processes without eliminating RNP granules in neural processes or decreasing AHA labeling. These data also suggest that these conditions allow local protein synthesis but minimize transport of somatically synthesized proteins into neural processes.

Visual conditioning increases local protein synthesis in the tectal neuropil

Using the conditions established above, we tested whether a visual conditioning protocol, known to induce protein synthesis-dependent behavioral plasticity *in vivo* (Shen et al., 2014), changes protein synthesis in the tectal neuropil, using the protocol in Figure 5*a*. The visual stimulus used for conditioning consisted of 1-cm-wide white bars on a dark background moving at 0.3 Hz in each of the four cardinal directions in pseudorandom order (Fig. 5*b*). We injected 5 mg/ml colchicine into the tectal ventricle 0.5 h before exposing animals to visual conditioning or ambient light (control) and then injected AHA, mixed with colchicine, immediately before visual conditioning to label proteins that were synthesized in response to visual conditioning. AHA was mixed with colchicine to avoid diluting colchicine with the AHA injection. Based on our observation that colchicine disrupted microtubules for up to 2 h after injection, animals were exposed to visual conditioning for a total of 1.5 h, starting 0.5 h after the first colchicine injection. This time window was intended to limit the contribution of somatic protein synthesis to the AHA fluorescence signal in the neuropil. To quantify newly synthesized proteins in neuronal processes in the tectal neuropil, we created a mask of the ROI based on NβT immunolabeling (Fig. 5*c*). We then determined the AHA fluorescence intensity in the NβT $^+$ ROI to capture only the AHA labeling within neuronal processes. Animals exposed to visual conditioning had 23 ± 8% greater AHA labeling in NβT $^+$ neuronal

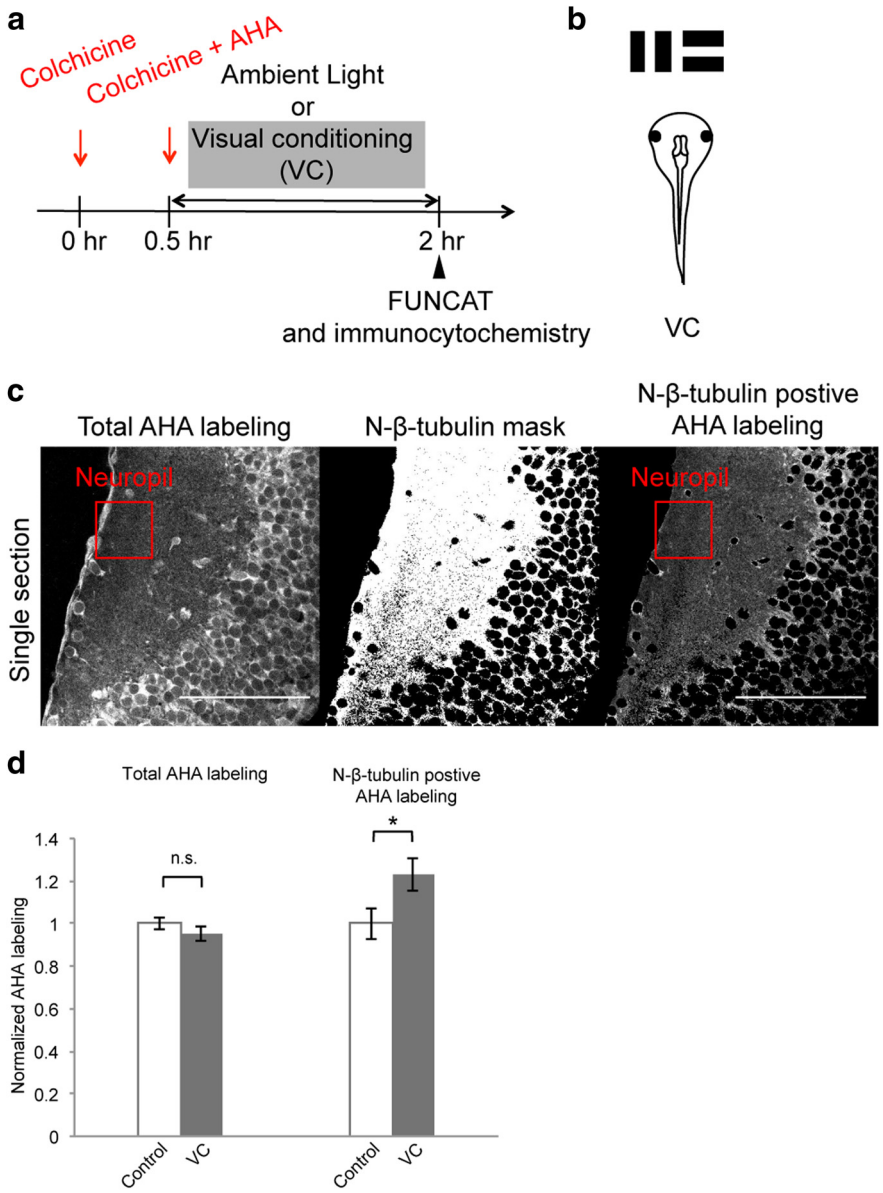

Figure 5. Visual conditioning increases local protein synthesis in the tectal neuropil. ***a***, Protocol to evaluate AHA labeling in the optic tectal neuropil of tadpoles presented with visual conditioning or ambient light. Tadpoles were injected in the midbrain ventricle with colchicine and then AHA in colchicine solution. Immediately after the AHA injection, animals were exposed to 1.5 h visual conditioning or ambient light. Animals were then fixed and their brains were processed for FUNCAT. ***b***, Schematic of tadpoles exposed to visual conditioning with moving bars. ***c***, Images of a single representative optical section of the left lobe of the tectum showing AHA labeling (left), a mask of NβT immunolabeling (middle), and AHA labeling within the NβT mask. The red box marks the area within the tectal neuropil where we measured AHA fluorescence intensity. ***d***, Normalized fluorescence intensity within the tectal neuropil of animals exposed to visual conditioning or ambient light (control). Visual conditioning increased AHA labeling in the tectal neuropil compared with control but did not result in detectable changes in global AHA labeling. Control: 1 ± 0.07, $n = 24$ animals; visual conditioning: 1.23 ± 0.08, $n = 26$ animals. $^{*}p < 0.05$, $^{**}p < 0.01$, Mann–Whitney *U* test. Error bars represent ± SEM. Scale bar, 100 μm.

processes compared with animals exposed to ambient light (Fig. 5*d*). In contrast, AHA labeling intensity measured in the same region of neuropil without the NβT mask was comparable in animals exposed to ambient light or conditioning (Fig. 5*d*). Our data indicate that visual conditioning increases protein synthesis in neuronal processes in the tectal neuropil.

FMRP knockdown increases protein synthesis in NPCs and neurons

We showed that visual conditioning increases protein synthesis in the tectal neuropil (Fig. 5), but the underlying mechanisms remain unclear. We are interested in testing whether the increase in local protein synthesis in response to visual conditioning is regulated by FMRP. First, we tested whether FMRP knockdown increases protein synthesis in the optic tectum by comparing the difference in AHA labeling over 1 and 3 h of AHA exposure. We knocked down FMRP by electroporating tectal cells with antisense FMOs, which reduce FMRP expression in *Xenopus* tectum (Faulkner et al., 2015). Control animals were electroporated with CMOs. After 2 d to allow knockdown, AHA was injected into the midbrain ventricle of tadpoles, they were fixed after 1 or 3 h, and their brains were processed for AHA labeling. We measured the fluorescence intensity of AHA labeling in the ventricular layer, which is populated by NPCs, in the neuronal cell body layer and in the neuropil in paired groups of animals that were treated with CMOs or FMOs from six clutches of tadpoles (Fig. 6*a*,*b*). The average fluorescence intensities of animals after 3 h AHA labeling were normalized to the average intensities of animals after 1 h AHA labeling from the same clutch. FMRP knockdown increased AHA labeling in NPCs, neuronal cell bodies, and neuropil compared with animals treated with CMOs (Fig. 6*c*; Table 3). These data indicate that FMRP knockdown increases newly synthesized proteins in somata and processes detected over 2 h exposure to AHA.

FMRP knockdown and visual conditioning increase local protein synthesis in the tectal neuropil

Next, we tested whether FMRP knockdown regulates protein synthesis in the tectal neuropil and whether the visual conditioning-dependent increase in newly synthesized proteins in the tectal neuropil is regulated by FMRP, using the protocol in Figure 7*a*. Animals were electroporated with either CMOs or FMOs. Two days later, we injected the midbrain ventricle with 5 mg/ml colchicine 0.5 h before visual conditioning and then AHA with colchicine immediately before visual conditioning, as described above. To determine whether visual conditioning affects protein synthesis in the tectal neuropil in the FMRP knockdown animals, we compared the AHA labeling in animals exposed to visual conditioning or ambient light (control) for 2 h (Fig. 7*a*). Visual conditioning significantly increased AHA labeling in the tectal neuropil of animals treated with CMOs. FMRP knockdown alone increased AHA labeling in the tectal neuropil compared with CMOs (Fig. 7*b*), but we did not see an additional increase in AHA labeling when we exposed FMRP knockdown tadpoles to visual conditioning (Fig. 7*b*). These

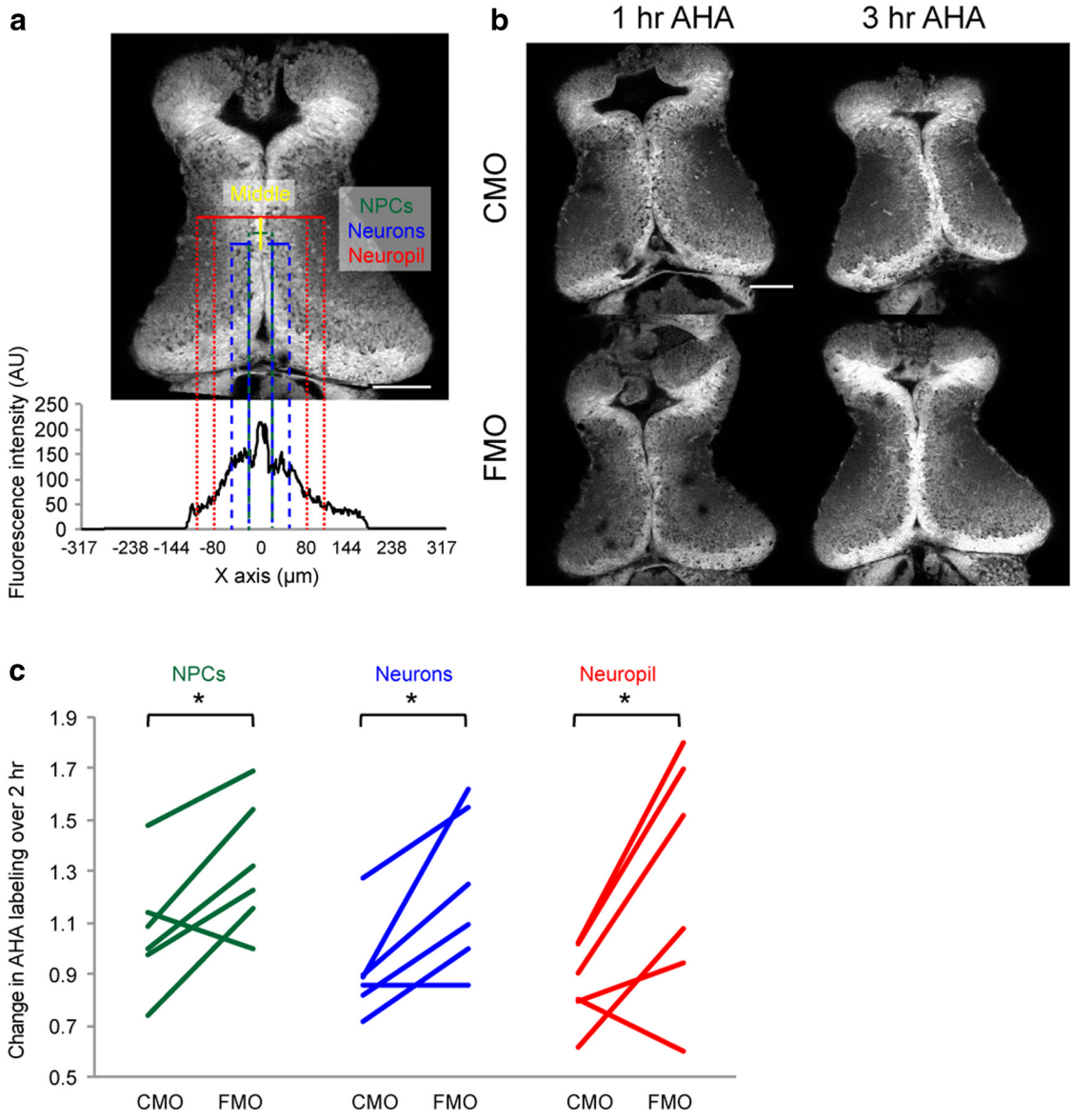

Figure 6. FMRP regulates protein synthesis in NPCs, neurons, and neuropil. ***a***, Quantification of AHA labeling in optic tectal cells. Top, Fluorescence intensity of AHA labeling was measured along horizontal (mediolateral) lines through the NPCs, neuronal cell body layer, and neuropil of the tectum. Positions of representative lines for analysis of AHA labeling intensity are shown superimposed on an image of a single optical section of the tectum from a tadpole labeled with AHA for 3 h. The vertical yellow line marks the tectal midline, the green and blue lines mark the NPC and neuronal cell body regions, respectively, and the red line marks neuropil regions. Bottom, Fluorescence intensity measurements of AHA labeling along a horizontal line from the lateral edges of the image through the cellular ROIs, as labeled in the image above. ***b***, Single optical sections of AHA labeling in FMO- or CMO-treated animals labeled with AHA for 1 or 3 h. ***c***, The change in AHA labeling intensity over 2 h in the NPCs (green), neuronal cell bodies (blue), and neuropil (red). Each line shows data from one experiment in which fluorescence intensity measurements were collected from two groups of tadpoles from the same clutch treated with CMOs or FMOs 2 d before labeling with AHA for 1 or 3 h. The AHA intensity ratios (3 h/1 h) from CMO- or FMO-treated animals from each independent experiment were paired for statistical analysis. FMRP knockdown increases protein translation in the NPCs, neuronal cell body layer, and neuropil. $n = 6$ independent experiments in total. $^*p < 0.05$, Wilcoxon's signed-rank test. Scale bar, 100 μm.

results indicate that both FMRP knockdown and visual conditioning increase protein synthesis in the neuropil. Together with previous work describing protein synthesis-dependent visual system plasticity (Shen et al., 2014), the data suggest that FMRP knockdown might affect visual system plasticity.

FMRP knockdown blocks maintenance of visual conditioning-induced behavioral plasticity

To determine the functional consequences of FMRP knockdown on protein synthesis-dependent visual system plasticity, we examined visual avoidance behavioral plasticity in FMRP knockdown animals. Tadpoles exhibit visual avoidance behavior in response to an approaching object (Dong et al., 2009; McKeown et al., 2013), and their rate of successful avoidance responses increases after animals receive conditioning visual stimulation (Shen et al., 2014). The behavior is quantified as an AI, the ratio of avoidance responses to encounters with an approaching visual stimulus (Shen et al., 2014).

Baseline avoidance behavior was tested 2 d after animals were electroporated with either CMOs or FMOs, and then animals were subjected to 1.5 h visual conditioning followed by avoidance behavior tests 2, 2.5, and 24 h after the onset of visual conditioning (Fig. 8*a*). We found no significant difference in baseline avoidance behavior before animals were exposed to visual condi-

Table 3. Change in AHA labeling over 2 h for FMO- and CMO-treated animals by clutch

	NPCs		Neurons		Neuropil		
Treatment	Mean ± SEM	Range	Mean ± SEM	Range	Mean ± SEM	Range	*n*
1							
CMO	1.48 ± 0.14	1.22–1.68	1.28 ± 0.07	1.17–1.40	1.02 ± 0.12	0.79–1.20	3
FMO	1.69 ± 0.02	1.68–1.71	1.55 ± 0.07	1.48–1.62	1.70 ± 0.06	1.64–1.76	2
2							
CMO	1.14 ± 0.12	1.03–1.26	0.86 ± 0.09	0.78–0.95	0.80 ± 0.06	0.74–0.86	2
FMO	1.00 ± 0.05	0.87–1.19	0.86 ± 0.03	0.75–0.96	0.60 ± 0.07	0.38–0.79	5
3							
CMO	0.75 ± 0.19	0.55–0.94	0.72 ± 0.14	0.58–0.87	0.62 ± 0.04	0.58–0.66	2
FMO	1.16 ± 0.27	0.89–1.42	1.00 ± 0.17	0.83–1.17	1.08 ± 0.39	0.69–1.47	2
4							
CMO	0.98 ± 0.23	0.53–1.27	0.82 ± 0.16	0.53–1.09	0.80 ± 0.13	0.57–1.02	3
FMO	1.23 ± 0.12	1.11–1.35	1.10 ± 0.10	1.00–1.20	0.95 ± 0.22	0.73–1.17	2
5							
CMO	1.00 ± 0.04	0.92–1.07	0.90 ± 0.04	0.86–0.99	1.02 ± 0.16	0.78–1.33	3
FMO	1.33 ± 0.02	1.31–1.34	1.26 ± 0.09	1.17–1.35	1.81 ± 0.08	1.73–1.88	2
6							
CMO	1.09	1.09	0.89	0.89	0.9	0.9	1
FMO	1.55 ± 0.05	1.45–1.57	1.63 ± 0.11	1.46–1.84	1.53 ± 0.12	1.39–1.77	3

Change in AHA labeling over 2 h for FMO- and CMO-treated animals by clutch. Data for Figure 6*c* are shown.

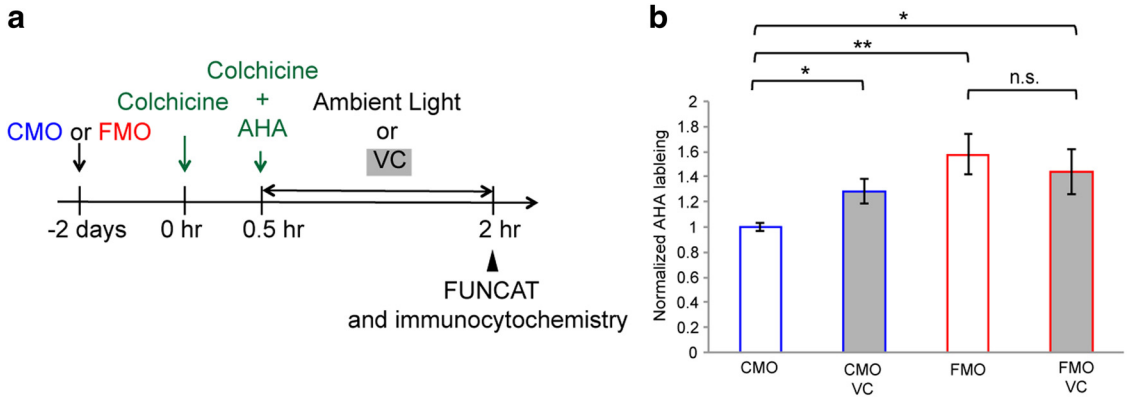

Figure 7. FMRP knockdown and visual conditioning (VC) increase local protein synthesis in the tectal neuropil. ***a***, Protocol to evaluate effects of FMRP knockdown and VC on AHA labeling in the optic tectal neuropil. Tadpoles were electroporated with CMOs or FMOs and 2 d later received ventricular injections of colchicine and AHA. Tadpoles were exposed to VC or ambient light (control) for 1.5 h and fixed, and their brains were processed for FUNCAT. AHA labeling was measured using a NβT mask. ***b***, Normalized AHA labeling measured in neuronal processes in tecta of FMO- or CMO-treated animals exposed to VC or ambient light (control). VC and FMRP knockdown each increase local protein synthesis. CMO control: 1 ± 0.03, $n = 14$ animals; CMO VC: 1.28 ± 0.1, $n = 14$ animals; FMO control: 1.58 ± 0.16, $n = 13$ animals; FMO VC: 1.44 ± 0.18, $n = 15$ animals. $^*p < 0.05$, $^{**}p < 0.01$, Steel–Dwass test. Error bars represent ± SEM.

tioning (AI: CMOs, 0.36 ± 0.02; FMOs, 0.39 ± 0.03). Control and FMRP knockdown animals showed comparable plasticity of the visual avoidance behavior immediately after visual conditioning (AI: CMOs, 0.49 ± 0.03; FMOs, 0.54 ± 0.03). CMO-treated animals maintained the plasticity for up to 24 h after visual conditioning (Fig. 8*b*,*c*), but the visual conditioning-induced behavioral plasticity was not maintained at the 24 h time point in FMRP knockdown animals (Fig. 8*d*,*e*). These data indicate that behavioral plasticity can be induced in FMRP knockdown animals, but the plasticity degrades in the absence of FMRP.

Discussion

Considerable evidence has shown the importance of newly synthesized mRNA and proteins in long-term synaptic plasticity and memory formation (Agranoff and Klinger, 1964; Agranoff et al., 1965; Lamprecht and LeDoux, 2004; Cajigas et al., 2010; West and Greenberg, 2011). Nevertheless, the underlying mechanisms of activity-induced protein synthesis-dependent synaptic plasticity are unclear. In this study, we optimized the spatial and temporal resolution of FUNCAT to allow systematic analysis of the role of FMRP in the regulation of local protein synthesis and experience-dependent behavioral plasticity in intact *Xenopus* tadpoles. We demonstrated that protein synthesis in the tectal neuropil increases in response to visual conditioning in the developing visual system and that both visual conditioning and FMRP regulate protein synthesis in tectal neuronal processes. Finally, using an assay of visual avoidance behavioral plasticity, we showed that FMRP knockdown does not interfere with induction of behavioral plasticity, but it blocks maintenance of plasticity. Together, we conclude that FMRP is important for visual conditioning-induced local protein synthesis and is required to maintain visual conditioning-dependent behavior plasticity.

Changes in local protein synthesis has been reported in response to different treatments, for example, BDNF and (*RS*)-3,5-dihydroxyphenylglycine (DHPG) *in vitro* (Huber et al., 2000; Aakalu et al., 2001; Dieterich et al., 2010), but, as a result of limited tools available for *in vivo* studies, few studies have investigated whether sensory input, such as visual experience, affects local protein synthesis in intact animals. Recently, several methods have been developed to visualize protein synthesis (Schmidt

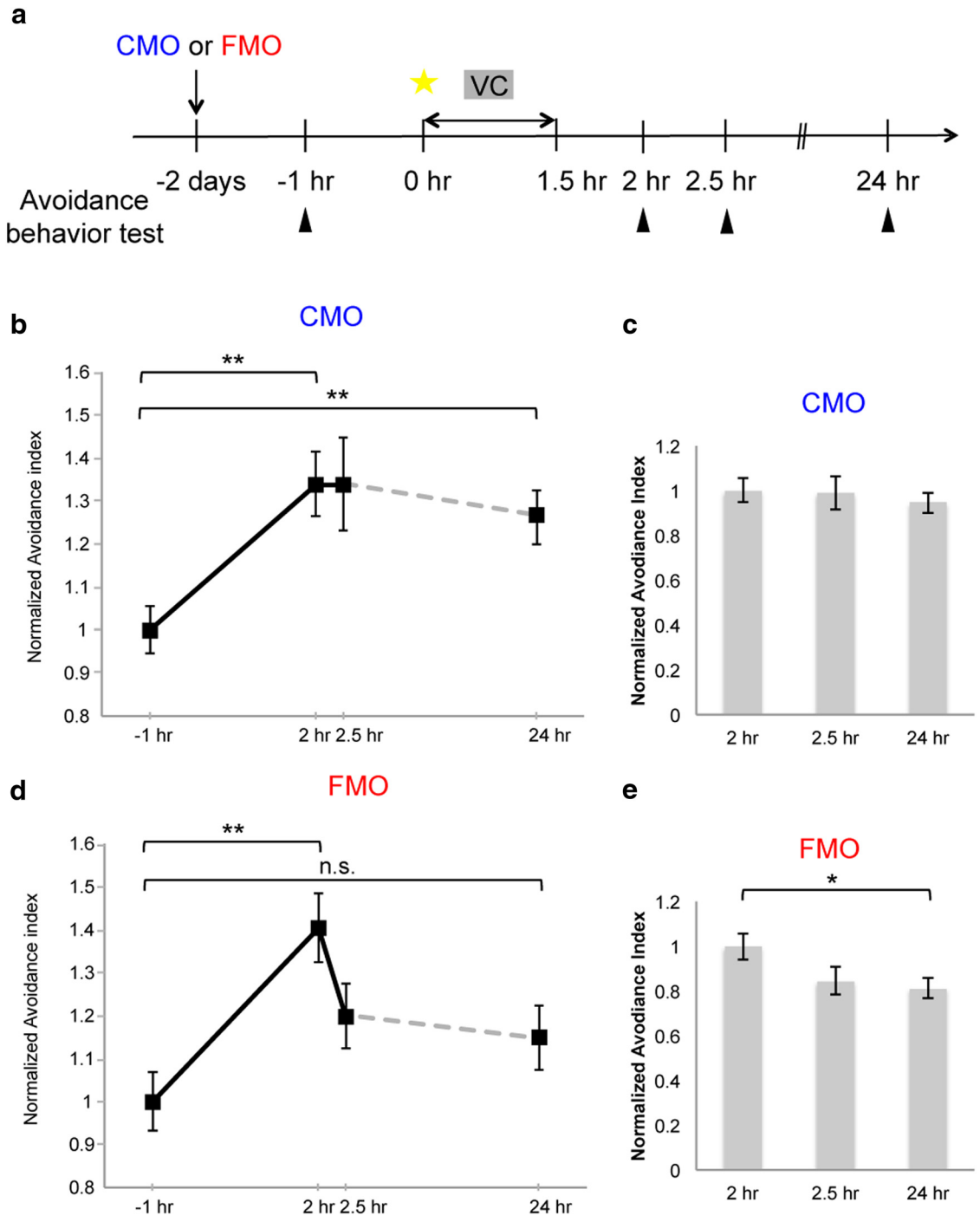

Figure 8. FMRP knockdown blocks maintenance of visual conditioning (VC)-dependent behavioral plasticity. ***a***, Protocol to evaluate the effect of FMRP knockdown on visual avoidance behavior. Animals were electroporated with CMOs or FMOs and 2 d later were assayed for baseline visual avoidance behavior at −1 h, exposed to VC for 1.5 h, and assayed for visual avoidance behavior 2, 2.5, and 24 h after VC started. Yellow star marks the time corresponding to AHA labeling shown in Figure 7*a*. ***b***, ***c***, VC-induced visual avoidance behavioral plasticity in CMO-treated animals was maintained for 24 h. ***d***, ***e***, VC-induced visual avoidance behavioral plasticity in FMO-treated animals, but the plasticity degraded over 24 h. AI values from each animal were either normalized to baseline at −1 h (***b***, ***d***) or normalized to the response 2 h after VC (***c***, ***e***). ***b***, ***d***, CMO: normalized AI, 1 ± 0.06, 1.34 ± 0.07, 1.34 ± 0.10, and 1.27 ± 0.06; $n = 17, 25, 22$, or 33 animals for tests at −1, 2, 2.5, or 24; FMO: normalized AI, 1 ± 0.07, 1.4 ± 0.08, 1.2 ± 0.08, or 1.15 ± 0.07; $n = 18, 18, 22$, or 33 animals for tests at −1, 2, 2.5, or 24 h. ***c***, ***e***, CMO: normalized AI, 1 ± 0.05, 0.99 ± 0.08, or 0.95 ± 0.05; FMO: normalized AI, 1 ± 0.06, 0.84 ± 0.06, or 0.81 ± 0.05. *$p < 0.05$, **$p < 0.01$, nonparametric comparisons for each pair using Wilcoxon's test. Error bars represent ± SEM.

et al., 2009; Dieterich et al., 2010; Ngo and Tirrell, 2011; Goodman et al., 2012; Hinz et al., 2012; Elliott et al., 2014). We improved the temporal resolution for detection of newly synthesized proteins in *X. laevis in vivo* to correspond to the time course of induction of protein synthesis-dependent visual avoidance plasticity. By treating animals with translational inhibitors or increasing translation with PTZ or FMRP knockdown, we showed that FUNCAT has sufficient sensitivity and dynamic range to detect increases and decreases in translation. Combining FUNCAT with immunolabeling different cell types enabled us to increase the cellular resolution of FUNCAT and demonstrate that NPCs are more active in protein synthesis than neurons.

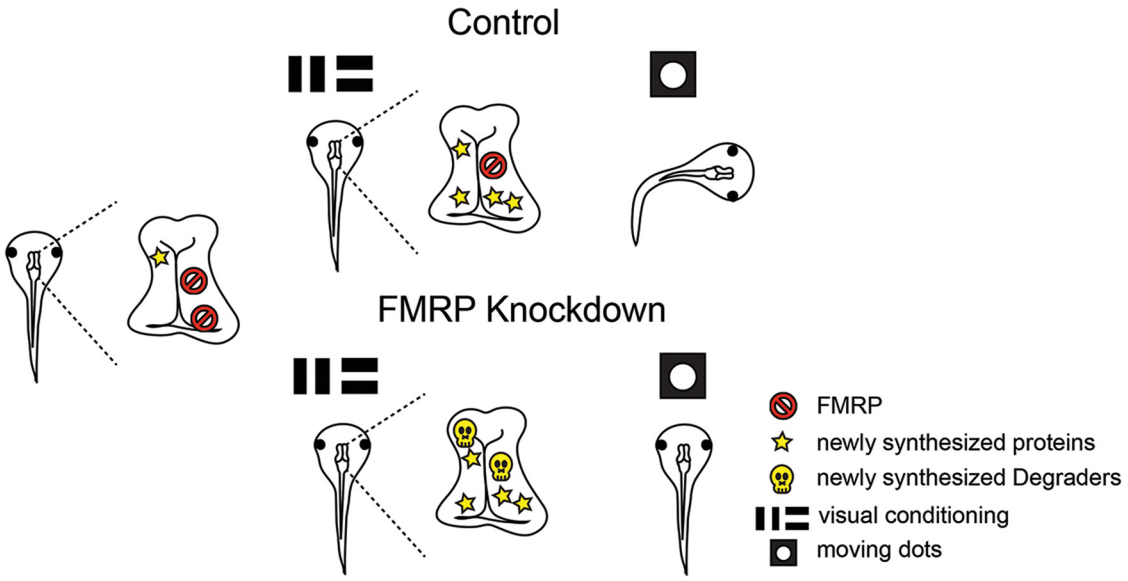

Figure 9. Model for changes in protein synthesis regulated by FMRP underlying visual conditioning-induced behavioral plasticity. Before visual conditioning, basal levels of protein synthesis (yellow stars) occurs in the presence of FMRP (red circle). Under control conditions, visual conditioning induces local protein synthesis and FMRP limits the synthesis of a Degrader protein (yellow skull), so behavioral plasticity is maintained in the presence of FMRP. With FMRP knockdown, visual conditioning induces both local protein synthesis and behavioral plasticity, comparable with conditioned control animals, but synthesis of Degrader, which is no longer suppressed by FMRP, disrupts maintenance of plasticity.

Significant spatial and temporal resolution of FUNCAT within neural processes *in vivo* is critical to examine the functions of FMRP and visual conditioning in protein synthesis-dependent behavioral plasticity. Previous studies distinguished local protein synthesis in neuronal processes from somatic protein synthesis by growing cells in microfluidic cell culture devices or by sparsely culturing neurons to segregate the processes from somata (Dieterich et al., 2010; Swanger et al., 2013; Taylor et al., 2013) and physically cutting them from the somata (Huber et al., 2000; Aakalu et al., 2001) or microperfusing drugs locally to minimize the contribution from the somata (Dieterich et al., 2010). These methods required sparse or guided growth of neurons, which limit applications *in vivo*. Others have used photoconvertible fluorescent proteins to examine axonal protein synthesis (Leung and Holt, 2008). Here, we minimized the contribution of somatically synthesized proteins in neuronal processes by interfering with microtubule-based transport using colchicine, which has been shown to block somatic transport of newly synthesized proteins (Fischer and Schmatolla, 1972). Although colchicine can block transport of RNP granules (Shan et al., 2003; Antar et al., 2005), we identified conditions in which microtubule structure is transiently and reversibly disrupted without affecting RNP localization in neural processes or protein synthesis in intact animals. With brief colchicine treatments, FUNCAT can be used to visualize locally synthesized proteins in neural processes *in vivo*. The tectal neuropil includes tectal cell dendrites and local axons, afferent inputs, and radial NPC processes extending to the pia. All of these processes include RNPs (Leung and Holt, 2008; Bestman and Cline, 2009). We measured AHA-labeling intensity within an ROI defined by an NβT mask to capture signals only in neuronal processes in the tectal neuropil and exclude signal from NPCs. By combining these strategies with a visual conditioning protocol shown previously to induce protein synthesis-dependent behavioral plasticity, we documented a visual conditioning-dependent increase in neuronal local protein synthesis in intact animals.

FMRP is thought to regulate synaptic plasticity by suppressing local translation of its target mRNAs (Weiler et al., 2004; Darnell and Klann, 2013; Sidorov et al., 2013). Previous studies have shown that both FMRP knockdown and knock-out increase newly synthesized proteins by ~20% (Qin et al., 2005; Dölen et al., 2007; Osterweil et al., 2010). We found 15–20% increase in newly synthesized protein in cell body layers of neurons and NPCs with FMRP knockdown and ~60% increase in local protein synthesis in the neuropil, indicating that FMRP regulates protein synthesis in both somata and processes in neurons and NPCs. The increase in local translation we observe is larger than reported in the knock-out mouse, possibly because our knockdown is acute. Visual conditioning and FMRP knockdown produced similar increases in local protein synthesis, and exposing FMRP knockdown animals to visual conditioning did not further increase local protein synthesis. We examined visual conditioning-induced behavioral plasticity in FMRP knockdown animals to see whether FMRP knockdown animals can still respond to visual conditioning with induced behavioral plasticity. The ability to track changes in avoidance behavior over time enabled us to investigate the dynamics in behavior plasticity. We found that FMRP knockdown animals are able to induce behavioral plasticity in response to visual conditioning, but the plasticity degrades over the following 24 h. These data indicate that FMRP knockdown does not impair protein synthesis necessary for induction of visual condition induced plasticity (Shen et al., 2014), for instance by saturating local protein synthesis machinery. They further indicate that FMRP is required for maintenance of the visually induced behavioral plasticity. Our data support a model in which visual conditioning-induced protein synthesis is required for conditioning-induced behavior plasticity and suggest that FMRP normally limits the synthesis of a Degrader protein, so that plasticity is maintained in the presence of FMRP. In the absence of FMRP, visual conditioning induces behavioral plasticity, comparable with conditioned control animals, but synthesis of Degrader protein, which is no longer suppressed by FMRP, then prevents the maintenance of plasticity (Fig. 9). This idea is distinct from the model of how FMRP is thought to affect mGluR-mediated LTD, in which mGluR activity induces the synthesis of

proteins required to maintain LTD, and FMRP limits their synthesis to cap the magnitude of LTD. In the absence of FMRP, synthesis of LTD proteins is not limited, and, consequently, the magnitude of mGluR-mediated LTD is greater than in controls (Huber et al., 2002; Bear et al., 2004). Application of this model to our system would result in greater magnitude behavioral plasticity than seen in CMO-treated animals. The common element of both models is that FMRP modulates the magnitude of long-lasting plasticity by limiting the synthesis of proteins that regulate the maintenance of plasticity (Fig. 9).

In summary, with improved spatiotemporal resolution of FUNCAT in intact animals, we showed that local protein synthesis increases in response to a behavioral plasticity-inducing visual conditioning protocol and demonstrate directly that FMRP knockdown increases protein synthesis in neuronal processes *in vivo*. Furthermore, using a visual avoidance assay, we demonstrate that FMRP is required to maintain long-term visuomotor behavioral plasticity. Our findings provide strong support for a role for FMRP in local protein synthesis-dependent behavioral plasticity and shed light on how behavioral plasticity mechanisms are regulated by FMRP through local protein synthesis.

References

Aakalu G, Smith WB, Nguyen N, Jiang C, Schuman EM (2001) Dynamic visualization of local protein synthesis in hippocampal neurons. Neuron 30:489–502. CrossRef Medline

Agranoff BW, Klinger PD (1964) Puromycin effect on memory fixation in the goldfish. Science 146:952–953. CrossRef Medline

Agranoff BW, Davis RE, Brink JJ (1965) Memory fixation in the goldfish. Proc Natl Acad Sci U S A 54:788–793. CrossRef Medline

Antar LN, Dictenberg JB, Plociniak M, Afroz R, Bassell GJ (2005) Localization of FMRP-associated mRNA granules and requirement of microtubules for activity-dependent trafficking in hippocampal neurons. Genes Brain Behav 4:350–359. CrossRef Medline

Bear MF, Huber KM, Warren ST (2004) The mGluR theory of fragile X mental retardation. Trends Neurosci 27:370–377. CrossRef Medline

Bestman JE, Cline HT (2009) The relationship between dendritic branch dynamics and CPEB-labeled RNP granules captured in vivo. Front Neural Circuits 3:10. CrossRef Medline

Bolte S, Cordelières FP (2006) A guided tour into subcellular colocalization analysis in light microscopy. J Microsc 224:213–232. CrossRef Medline

Cajigas IJ, Will T, Schuman EM (2010) Protein homeostasis and synaptic plasticity. EMBO J 29:2746–2752. CrossRef Medline

Darnell JC, Klann E (2013) The translation of translational control by FMRP: therapeutic targets for FXS. Nat Neurosci 16:1530–1536. CrossRef Medline

Dent JA, Polson AG, Klymkowsky MW (1989) A whole-mount immunocytochemical analysis of the expression of the intermediate filament protein vimentin in *Xenopus*. Development 105:61–74. Medline

Dieterich DC, Hodas JJ, Gouzer G, Shadrin IY, Ngo JT, Triller A, Tirrell DA, Schuman EM (2010) In situ visualization and dynamics of newly synthesized proteins in rat hippocampal neurons. Nat Neurosci 13:897–905. CrossRef Medline

Dölen G, Osterweil E, Rao BS, Smith GB, Auerbach BD, Chattarji S, Bear MF (2007) Correction of fragile X syndrome in mice. Neuron 56:955–962. CrossRef Medline

Dong W, Lee RH, Xu H, Yang S, Pratt KG, Cao V, Song YK, Nurmikko A, Aizenman CD (2009) Visual avoidance in *Xenopus* tadpoles is correlated with the maturation of visual responses in the optic tectum. J Neurophysiol 101:803–815. Medline

Elliott TS, Townsley FM, Bianco A, Ernst RJ, Sachdeva A, Elsässer SJ, Davis L, Lang K, Pisa R, Greiss S, Lilley KS, Chin JW (2014) Proteome labeling and protein identification in specific tissues and at specific developmental stages in an animal. Nat Biotechnol 32:465–472. CrossRef Medline

Faulkner RL, Wishard TJ, Thompson CK, Liu HH, Cline HT (2015) FMRP regulates neurogenesis in vivo in *Xenopus laevis* tadpoles. eNeuro 2:e0055. Medline

Feng Y, Gutekunst CA, Eberhart DE, Yi H, Warren ST, Hersch SM (1997) Fragile X mental retardation protein: nucleocytoplasmic shuttling and association with somatodendritic ribosomes. J Neurosci 17:1539–1547. Medline

Ferreira TA, Blackman AV, Oyrer J, Jayabal S, Chung AJ, Watt AJ, Sjöström PJ, van Meyel DJ (2014) Neuronal morphometry directly from bitmap images. Nat Methods 11:982–984. CrossRef Medline

Fischer HA, Schmatolla E (1972) Axonal transport of tritium-labeled putrescinein the embryonic visual system of zebrafish. Science 176:1327–1329. CrossRef Medline

Gabel LA, Won S, Kawai H, McKinney M, Tartakoff AM, Fallon JR (2004) Visual experience regulates transient expression and dendritic localization of fragile X mental retardation protein. J Neurosci 24:10579–10583. CrossRef Medline

Gaete M, Muñoz R, Sánchez N, Tampe R, Moreno M, Contreras EG, Lee-Liu D, Larraín J (2012) Spinal cord regeneration in Xenopus tadpoles proceeds through activation of Sox2-positive cells. Neural Dev 7:13. CrossRef Medline

Gandhi RM, Kogan CS, Messier C, Macleod LS (2014) Visual-spatial learning impairments are associated with hippocampal PSD-95 protein dysregulation in a mouse model of fragile X syndrome. Neuroreport 25:255–261. CrossRef Medline

Goodman CA, Pierre P, Hornberger TA (2012) Imaging of protein synthesis with puromycin. Proc Natl Acad Sci U S A 109:E989; author reply E990. Medline

Harlow EG, Till SM, Russell TA, Wijetunge LS, Kind P, Contractor A (2010) Critical period plasticity is disrupted in the barrel cortex of FMR1 knockout mice. Neuron 65:385–398. CrossRef Medline

Hinz FI, Dieterich DC, Tirrell DA, Schuman EM (2012) Non-canonical amino acid labeling in vivo to visualize and affinity purify newly synthesized proteins in larval zebrafish. ACS Chem Neurosci 3:40–49. CrossRef Medline

Huber KM, Kayser MS, Bear MF (2000) Role for rapid dendritic protein synthesis in hippocampal mGluR-dependent long-term depression. Science 288:1254–1257. CrossRef Medline

Huber KM, Gallagher SM, Warren ST, Bear MF (2002) Altered synaptic plasticity in a mouse model of fragile X mental retardation. Proc Natl Acad Sci U S A 99:7746–7750. CrossRef Medline

Kéri S, Benedek G (2011) Fragile X protein expression is linked to visual functions in healthy male volunteers. Neuroscience 192:345–350. CrossRef Medline

Kim H, Gibboni R, Kirkhart C, Bao S (2013) Impaired critical period plasticity in primary auditory cortex of fragile X model mice. J Neurosci 33:15686–15692. CrossRef Medline

Kogan CS, Bertone A, Cornish K, Boutet I, Der Kaloustian VM, Andermann E, Faubert J, Chaudhuri A (2004) Integrative cortical dysfunction and pervasive motion perception deficit in fragile X syndrome. Neurology 63:1634–1639. CrossRef Medline

Kwon H, Menon V, Eliez S, Warsofsky IS, White CD, Dyer-Friedman J, Taylor AK, Glover GH, Reiss AL (2001) Functional neuroanatomy of visuospatial working memory in fragile X syndrome: relation to behavioral and molecular measures. Am J Psychiatry 158:1040–1051. CrossRef Medline

Laggerbauer B, Ostareck D, Keidel EM, Ostareck-Lederer A, Fischer U (2001) Evidence that fragile X mental retardation protein is a negative regulator of translation. Hum Mol Genet 10:329–338. CrossRef Medline

Lamprecht R, LeDoux J (2004) Structural plasticity and memory. Nat Rev Neurosci 5:45–54. CrossRef Medline

Leung KM, Holt CE (2008) Live visualization of protein synthesis in axonal growth cones by microinjection of photoconvertible Kaede into *Xenopus* embryos. Nat Protoc 3:1318–1327. CrossRef Medline

Li J, Cline HT (2010) Visual deprivation increases accumulation of dense core vesicles in developing optic tectal synapses in *Xenopus laevis*. J Comp Neurol 518:2365–2381. CrossRef Medline

Li Z, Zhang Y, Ku L, Wilkinson KD, Warren ST, Feng Y (2001) The fragile X mental retardation protein inhibits translation via interacting with mRNA. Nucleic Acids Res 29:2276–2283. CrossRef Medline

Ling SC, Fahrner PS, Greenough WT, Gelfand VI (2004) Transport of *Drosophila* fragile X mental retardation protein-containing ribonucleoprotein granules by kinesin-1 and cytoplasmic dynein. Proc Natl Acad Sci U S A 101:17428–17433. CrossRef Medline

Liu-Yesucevitz L, Bassell GJ, Gitler AD, Hart AC, Klann E, Richter JD, Warren ST, Wolozin B (2011) Local RNA translation at the synapse and in disease. J Neurosci 31:16086–16093. CrossRef Medline

Martin KC, Barad M, Kandel ER (2000) Local protein synthesis and its role in synapse-specific plasticity. Curr Opin Neurobiol 10:587–592. CrossRef Medline

McKeown CR, Sharma P, Sharipov HE, Shen W, Cline HT (2013) Neurogenesis is required for behavioral recovery after injury in the visual system of Xenopus laevis. J Comp Neruol 521:2262–2278. CrossRef Medline

Moody SA, Miller V, Spanos A, Frankfurter A (1996) Developmental expression of a neuron-specific beta-tubulin in frog (*Xenopus laevis*): a marker for growing axons during the embryonic period. J Comp Neurol 364:219–230. CrossRef Medline

Ngo JT, Tirrell DA (2011) Noncanonical amino acids in the interrogation of cellular protein synthesis. Acc Chem Res 44:677–685. CrossRef Medline

Osterweil EK, Krueger DD, Reinhold K, Bear MF (2010) Hypersensitivity to mGluR5 and ERK1/2 leads to excessive protein synthesis in the hippocampus of a mouse model of fragile X syndrome. J Neurosci 30:15616–15627. CrossRef Medline

Plucińska G, Paquet D, Hruscha A, Godinho L, Haass C, Schmid B, Misgeld T (2012) In vivo imaging of disease-related mitochondrial dynamics in a vertebrate model system. J Neurosci 32:16203–16212. CrossRef Medline

Qin M, Kang J, Burlin TV, Jiang C, Smith CB (2005) Postadolescent changes in regional cerebral protein synthesis: an in vivo study in the FMR1 null mouse. J Neurosci 25:5087–5095. CrossRef Medline

Santoro MR, Bray SM, Warren ST (2012) Molecular mechanisms of fragile X syndrome: a twenty-year perspective. Annu Rev Pathol 7:219–245. CrossRef Medline

Schmidt EK, Clavarino G, Ceppi M, Pierre P (2009) SUnSET, a nonradioactive method to monitor protein synthesis. Nat Methods 6:275–277. CrossRef Medline

Shan J, Munro TP, Barbarese E, Carson JH, Smith R (2003) A molecular mechanism for mRNA trafficking in neuronal dendrites. J Neurosci 23:8859–8866. Medline

Shen W, Liu HH, Schiapparelli L, McClatchy D, He HY, Yates JR 3rd, Cline HT (2014) Acute synthesis of CPEB is required for plasticity of visual avoidance behavior in *Xenopus.* Cell Rep 6:737–747. CrossRef Medline

Sidorov MS, Auerbach BD, Bear MF (2013) Fragile X mental retardation protein and synaptic plasticity. Mol Brain 6:15. CrossRef Medline

Swanger SA, He YA, Richter JD, Bassell GJ (2013) Dendritic GluN2A synthesis mediates activity-induced NMDA receptor insertion. J Neurosci 33:8898–8908. CrossRef Medline

Taylor AM, Wu J, Tai HC, Schuman EM (2013) Axonal translation of beta-catenin regulates synaptic vesicle dynamics. J Neurosci 33:5584–5589. CrossRef Medline

Till SM, Wijetunge LS, Seidel VG, Harlow E, Wright AK, Bagni C, Contractor A, Gillingwater TH, Kind PC (2012) Altered maturation of the primary somatosensory cortex in a mouse model of fragile X syndrome. Hum Mol Genet 21:2143–2156. CrossRef Medline

Wang Y, Sakano H, Beebe K, Brown MR, de Laat R, Bothwell M, Kulesza RJ Jr, Rubel EW (2014) Intense and specialized dendritic localization of the fragile X mental retardation protein in binaural brainstem neurons: a comparative study in the alligator, chicken, gerbil, and human. J Comp Neurol 522:2107–2128. Medline

Weiler IJ, Spangler CC, Klintsova AY, Grossman AW, Kim SH, Bertaina-Anglade V, Khaliq H, de Vries FE, Lambers FA, Hatia F, Base CK, Greenough WT (2004) Fragile X mental retardation protein is necessary for neurotransmitter-activated protein translation at synapses. Proc Natl Acad Sci U S A 101:17504–17509. CrossRef Medline

West AE, Greenberg ME (2011) Neuronal activity-regulated gene transcription in synapse development and cognitive function. Cold Spring Harbor Perspect Biol 3(6). CrossRef

Yang S, Yang S, Park JS, Kirkwood A, Bao S (2014) Failed stabilization for long-term potentiation in the auditory cortex of FMR1 knockout mice. PLoS One 9:e104691. CrossRef Medline